Robust Optimization-Based Coronary Artery Labeling From X-Ray Angiograms

Xinglong Liu, Fei Hou, Hong Qin, and Aimin Hao

***Abstract*—In this paper, we present an efficient robust labeling method for coronary arteries from X-ray angiograms based on energy optimization. The fundamental goal of this research is to facilitate the analysis and diagnosis of interventional surgery in the most efficient way, and such effort could also improve the performance during doctor training, and surgery simulation and planning. Compared to the prior state-of-the-art, our method is much more robust to resist noises and is tolerant to even incomplete data because of the *"built-in"* nature of global optimization. We start with a fully parallelized algorithm based on Hessian matrix to extract the tubular structure from the X-ray angiograms as vessel candidates. Then, instead of using the candidates directly, we use the grow cut (Vezhnevets and V. Konouchine, Growcut: Interactive multi-label N-D image segmentation by cellular automata, in Proc. of Graphicon, 2005, pp. 150–156.) method, which is similar to graph cut (Boykov *et al.*, Fast approximate energy minimization via graph cuts, *IEEE Trans. Pattern Anal. Mach. Intell.*, vol. 23, no. 11, pp. 1222–1239, Nov. 2001.)but with better performance to extract the precise vessel structure from the images. Next, we use the fast marching method with second derivatives and cross neighbors to extract the accurate skeleton segments. After that, we propose an efficient method based on iterative closest point (Z. Zhang, Iterative point matching for registration of free-form curves and surfaces, *Int J. Comput. Vis.*, vol. 13, no. 2, pp. 119–152, 1994.) to organize the skeleton segments by treating the continuity and similarity as extra constraints. Finally, we formulate the vessel labeling problem as an energy optimization problem and solve it using belief propagation. We also demonstrate several typical applications including flow velocity estimation, heart beat estimation, and vessel diameter estimation to show its practical uses in clinical diagnosis and treatment. Our experiments exhibit the correctness and robustness, as well as the high performance of our algorithm. We envision that our system would be of high utility for diagnosis and therapy to treat vessel-related diseases in a clinical setting in the near future.**

***Index Terms*—Coronary artery, energy optimization, X-ray angiograms.**

I. Introduction

THE morbidity of cardiovascular disease (CVD) is rapidly increasing over the past few decades. CVD is the leading cause of deaths in both developed and developing countries. For example, it accounts for 17% of overall deaths in the USA [4], [5]. In Singapore, one out of three deaths are due to heart disease or stroke [6]. Because of the gradually-aging population in the world, the percentage of CVD patients is expected to dramatically increase [7] in the near future. The golden standard for diagnosis of CVD is X-ray coronary angiography. Reading and analyzing angiograms accurately is a compulsory course for fresh physicians involved in the intervention surgery or for the diagnosis of heart diseases. Accurate coronary artery segmentation and recognition are imperative for both cardiologists-in-training and medical practitioners, toward high-precision diagnosis, surgery planning, and treatment. This paper's originality hinges upon our efficient solution to extract the coronary arteries and recognize each artery with known labels. Besides, we apply our method in practical cases, gleaning all the important information from X-ray angiograms, which will in turn provide more quantitative guidance for later treatments.

Although various researches have been done, there are still some unsolved challenges currently. First, the angiograms are with low image quality, sometimes incomplete, making it difficult to extract accurate structures. Second, current methods are time-consuming, facing tremendous amount of angiograms produced daily. Third, the skeleton organization of current methods is usually based on either prior knowledge or geometrical structures and may not ensure a globally-optimized solution. Finally, the current methods calculate parameters of coronary arteries, such as flow velocity simply at the pixel level from acquired images without considering the global vessel structures and the structure relationship among images, which is not only wasting high-level more valuable information available in acquired images, but also far from being accurate.

To overcome the aforementioned shortcomings, we present an efficient and robust vessel extraction and labeling method in this paper, and explore several applications using the proposed method, including flow-velocity estimation, heart-beat rate estimation, etc. Compared to previous methods, our method is more robust to resist noise and to handle even incomplete data. The pipeline is shown in Fig. 1 consisting four stages: vessel and skeleton extraction (see Section III), vessel organization (see Section IV), tree structure labeling (see Section V), and application (see Section VII). First, we design a parallel algorithm based on Hessian matrix [8] to extract candidate vessels and make use of the grow cut [1] method based on cellular automata to further process the candidates for more accurate foreground coronary arteries. Then, we propose an iterative distance and similarity evaluation method based on iterative closest point (ICP) with the property of optimization to organize the extracted vessel skeleton into segments. After that, all

Manuscript received February 21, 2015; revised July 9, 2015 and September 1, 2015; accepted September 24, 2015. Date of publication October 1, 2015; date of current version December 6, 2016. *(corresponding author: Fei Hou.)*

X. Li and A. Hao are with the State Key Laboratory of Virtual Reality Technology and Systems, Beihang University, Beijing 100191, China (e-mail: liu3xing3long@163.com; ham_buaa@163.com).

F. Hou is with the School of Computer Engineering, Nanyang Technological University, Singapore 639798, and also with the State Key Laboratory of Virtual Reality Technology and Systems, Beihang University, Beijing 100191, China (e-mail: houfei@buaa.edu.cn).

H. Qin is with the Department of Computer Science, Stony Brook University, Stony Brook, NY 11794 USA (e-mail: qin@cs.stonybrook.edu).

Color versions of one or more of the figures in this paper are available online at http://ieeexplore.ieee.org.

Digital Object Identifier 10.1109/JBHI.2015.2485227

2168-2194 © 2015 IEEE. Personal use is permitted, but republication/redistribution requires IEEE permission.
See http://www.ieee.org/publications_standards/publications/rights/index.html for more information.

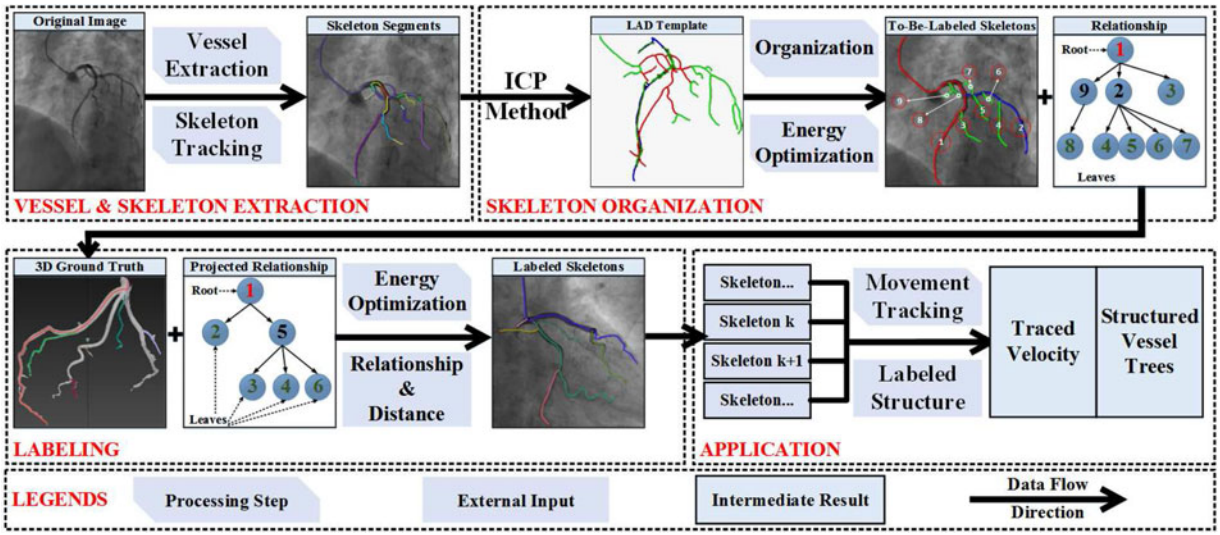

Fig. 1. Pipeline of our method consisting of four steps. Inputs are X-ray angiograms and one 3-D coronary artery model, while outputs are labeled skeletons with traced diameters, flow speed, and heart rate. Legends are given to indicate different meanings of colors and shapes.

vessel segments will be organized as well-structured trees. Then, we formulate the labeling problem of the organized skeletons into an energy optimization problem, and solve it using the belief propagation (BP). Finally, we apply our method to several practical estimation problems to facilitate a better diagnosis and treatment. The main contributions of our work include:

1) We develop an efficient parallelized vessel extraction and thinning method using Hessian matrix as well as the grow cut method. One advantage is that, at the image level, we take into consideration the probability and the continuity of each pixel/voxel belonging to vessels.
2) We develop an efficient, iterative distance, and similarity evaluation method based on ICP. We propose a framework based on this new descriptor to organize the extracted vessel skeletons into well structured trees, greatly simplifying the labeling problem at little performance loss.
3) We develop a novel labeling method based on global energy optimization, being solved using BP with *distance* and *topology* constraints, which is robust to noisy and incomplete data from images.
4) We explore several typical practical applications using the newly-proposed method to extract the physiological parameters from the X-ray angiograms, automatically.

II. Related Work

Our work relates to vessel extraction, skeleton tracking, energy optimization, etc. We now briefly review them in the following categories.

Vessel and Skeleton Extraction. The vessel extraction methods can be classified into different categories (See [9]). In addition, researchers focussed more on energy-based segmentation methods with combination of many classical methods. Salazar *et al.* [10] proposed a vessel segmentation method for retinal images based on energy optimization by combining the well known graph cut method with the classical optic disc method. Hoover *et al.* [11] used a mathematical filter to offer a broad range of vessel enhancement, and Li *et al.* [12] conducted this task using a nonlinear filter. Frangi *et al.* [8] used the eigenvalues of Hessian matrix to extract the tube-like structures from X-ray images. Condurache *et al.* [13] used this method while adding a hysteresis thresholding method to purify the extracted data, which is not robust to handle blurry images. Zhang *et al.* [14] proposed a novel extension of the matched filter approach, which is composed of a zero-mean Gaussian function and the first-order derivative of Gaussian. Typically, vessels extracted from angiograms are quite complicated. Centerline extraction for vessels is essential for both data simplification and further processing. Zhang *et al.* [15] proposed a two-step thinning method based on the structure analysis of the candidate vessel structures. Van *et al.* [16] and Hassouna *et al.* [17] proposed methods based on Eikonal equation and fast marching method to find vessel skeletons. Yet, they could not process isolated vessel segments.

Vessel Labeling. Labeling coronary arteries, focusing both on 2-D such as X-ray angiograms, and 3-D such as CT images, aims to offer semantic information corresponding to geometric structures. Ezquerra *et al.* [18] proposed a model-guided method automatically labeling vascular structures in the coronary angiographic images. They compared a feature graph with a symbolic graph based on feature correspondence, which is local and ignores the global nature. Haris *et al.* [19] proposed a segmentation and labeling method for coronary arteries based on artery tracking, morphological tools of homotopy modification, and watersheds. However, their method is not automatic and needs user interactions. Yang *et al.* [20] proposed a two-step matching algorithm, including main branch identification and all segments labeling based on 3-D ground truth models to label the coronary from the computed tomographic angiography. Throughout all labeling techniques, most are based on features which may not only cause mistakes due to blurry images, but also be unable to the achieve globally optimized results.

Optimization Techniques. Optimization techniques are widely used in various areas, such as image restoration, 3-D reconstruction, etc. Geman *et al.* [21] first proposed the classical theories of Markov random field (MRF), Gibbs Sampling, and maximum a posteriori estimate. Lafferty *et al.* [22] proposed the conditional random field (CRF), providing a tool for structural classification and prediction. Meanwhile, BP was proposed by Pearl [23] to solve the optimization problems in MRF. Ever since the inception of BP, various methods for improving its performance [24], as well as speeding up the method [25] have been proposed, which indicates its important role in energy optimization theory. Besides BP, graph cut is widely used in computer vision, including image segmentation [26], stereo disparity, and motion [2]. In [2], Boykov *et al.* presented an efficient α-expansion and α–β swap algorithm for metric energy minimization based on graph cut. Kolmogorov *et al.* [27] introduced the characteristics of the energy function which could be minimized by graph cut and conducted the genetic construction of the minimization function. Many extensions for graph cut have been proposed such as grab cut [28], etc. Despite the typical methods, Vezhnevets [1] proposed a method called grow cut which is similar to the graph cut, but is based on cellular automata with better performance.

Practical Applications. As with the applications in medical image analysis, Liu *et al.* [29] have proposed a method based on the energy optimization to extract the shape, motion from X-ray angiograms at different views. As relevant technologies advance, more sensors and instruments have been applied to measure the physiological parameters in coronary arteries, which facilitates the computational fluid dynamics (CFD). Tremendous progresses have been made in applying image-based CFD simulation techniques to elucidate the effects of hemodynamics in vascular pathophysiology toward the initialization and progression of CAD [30].

III. Vessel and Skeleton Extraction

Given X-ray angiograms, we design an efficient algorithm with the help of GPU for extracting the enhanced images as vessel candidates. After that, we use grow cut method which is based on cellular automata to select *foreground (vessels)* from vessel candidates with the knowledge from known *foreground*, *background,* and vessel continuity. At last, we apply the multi-stencils fast marching method with second derivative and cross neighbors to track the skeletons from segmented vessels. The final vessels as well as their skeletons are shown in Fig. 2.

A. Vessel Extraction

Original angiograms captured by X-ray machines are usually with low contrast, high dynamic range, and low lumen. To extract vessels from such images, we devise a global optimization method consisting of three steps, vessel enhancement, Hessian based vessel candidate extraction and globally-optimized precise extraction based on grow cut. The pipeline is described in Fig. 3.

1) Angiogram Enhancement: We first apply the enhancement of radiography based on Musicale Retinex with Color restoration (MSRCR) [31] method, since it can can combat these artifacts while keeping the edges sharp with low computational cost. This step is very important, since it is a base for further processing. Without this step, the images processed in the next step will be full of small artifacts, and some of which might be easy to be smoothed but many others are hard to distinguish. Then, we use the gain/offset method to fix the negative values. After the preprocessing procedure, original images are enhanced in contrast and lumen, providing better basis for vessel extraction.

2) Candidates From Hessian Matrix: The filter [8] based on Hessian matrix affords a good start of extracting the tubular structures for segmentation and improving the efficiency via GPU acceleration. Besides, the filtered values denote the corresponding probability for each pixel belonging to the vessels, making it convenient to add further process to ensure the continuity constrains. We convolve original images by Gaussian filters with different σ which are related to maximum vessel

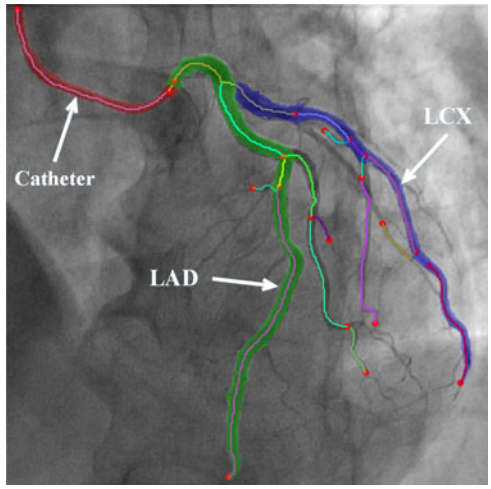

Fig. 2. Results of vessel and skeleton extraction. Catheter, LAD, and LCX branch are identified. Different colors correspond to different segments. Round filled circles identify bifurcations and distal points.

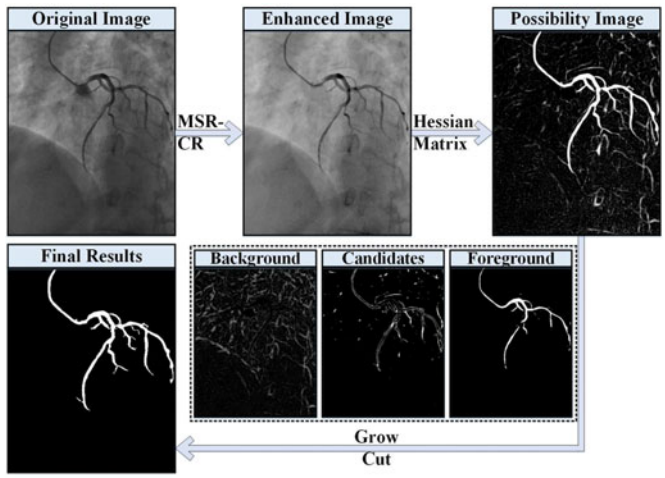

Fig. 3. Pipeline of vessel extraction. We use Hessian matrix to extract the vascular candidates from MSRCR-enhanced images, and classify them into three categories which are the inputs for grow cut to produce the final segmentations.

size of the image, and then, we normalize the convolved image using corresponding σ for further process.

In our application, for every angiogram among the imaging sequence and for every specified σ, our parallelized extraction method consists of the following steps. First, we build the Gaussian kernel mask depending on σ on the CPU side and transfer them into GPU. Second, we convolve the entire image using this Gaussian kernel and each pixel point on the image corresponds to one CUDA kernel. Third, we extract the eigenvalues and eigenvectors and compute the coefficients for each point's Hessian matrix. This is also done per kernel on GPU. Fourth, we use a double swap buffer on GPU to compute the possibility of being part of vessel structures for each pixel (refer to (15) of [8] for details). In all the procedures, except initialization, data are processed on the GPU side and stored for further process.

3) Precise Results Using grow cut: Filtered values from Hessian matrix are discrete in isolation without any knowledge of adjacency information. Simply using threshold can not extract satisfactory results from Hessian matrix. Therefore, Hessian matrix together with grow cut are used to guarantee more purified extraction results from the images. Hessian matrix is a good start for extracting the tubular structures and easy to be parallelized. However, Hessian is more focused on local "pixel" level on images, while grow cut could use the output of Hessian as an input and take neighboring information of current local pixel into consideration. These two methods are pair-wisely used to ensure the continuity, as well as the tubular feature of current pixel on the images. Grow cut [1] is an alternative to graph cut, yet with much better performance. This method can be regarded as having a biological metaphor that each image pixel is formulated as a cell of certain type. These cells can be *foreground*, *background*, *undefined,* or others. As the algorithm proceeds, these cells compete to dominate the image domain. The ability of the cells to spread is related to the image pixel intensity.

Based on the probability image acquired from the GPU-accelerated Hessian, we divide the candidates on the image into three categories: *background*, *foreground (vessel)*, and *undefined* pixels. For all pixels p on the image, the processing stage mainly comprises the following steps. First, current state and weighted strength from last iteration are saved. Second, for all neighbours q of pixel p under force F and strength S, we will compute the new strength through $F \times S$ and replace the old one if it is smaller. Third, all pixels on the image will be assigned with a label by 0 and 1, indicating the *background* and *foreground*, respectively. Fourth, we collect the *foreground* pixels as vessel segments and calculate the length (i.e., number of points) of each segment. Finally, segments whose number of points are smaller than a given value are omitted, and in this way, we can obtain clear vessel images as the Final Results in Fig. 3.

B. Skeleton Extraction

Vessel skeletonization is essential for data simplification. The Fast Marching method [32], [17] with second derivatives and cross neighbors provides a precise way to extract the skeletons.

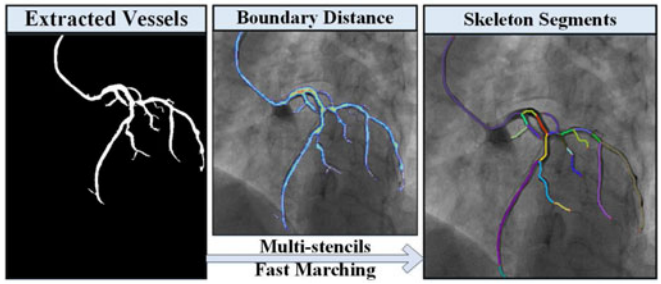

Fig. 4. Pipeline of the skeleton extraction. Multistencils fast marching is used with cross neighbours and second derivatives to improve the accuracy.

As illustrated in Fig. 4, we extract the accurate skeleton of the objects represented by binary images using the fast marching distance transform. First, we compute the distance map for the whole binary image (see Line 5, Algorithm 1). Second, we trace the shortest path from the start point to the source point using Runge–Kutta method in the distance map (see Line 11, Algorithm 1). Finally, we organize and split the traced points into the line segments (see Line 12, Algorithm 1). With the help of both second derivatives and cross neighbors, we obtain segmented skeletons more accurately. Meanwhile, we extracted the diameters for each skeleton point during the distance transform. The tracked skeleton segments have been shown in Fig. 2.

IV. Vessel Organization

In principle, extracted vessel skeletons are messy, less-accurate segments consisting of many pixels which may not exhibit well-behaved structures, not suitable for the immediate labeling. Since the importance of coronary branches is different (e.g., LAD and LCX are more important since they are root branches, mislabeling them would cause all the following subsequent labeling wrong); here, we adopted a two-step procedure based on the prior knowledge to first extract the most important two branches in the coronary arteries, called vessel organization (see Section IV) problem and tree structure labeling (see Section V) problem. In the first step, we organize the messy skeletons, transforming them into well-organized tree structures with an ICP-based similarity term. We select ICP as the core of the similarity term for its high efficiency. Thus, this step only consumes a little in terms of temporal cost, yet highly simplifies the labeling problem and increases the accuracy. In the second step, we compute optimized labeling results, focusing mainly on LAD (left anterior descending), LCX (left circumflex), OM (obtuse marginal) and D (diagonal) branch. We put different emphasis on different branches, since they may have different levels of significance during labeling. The pipeline of organizing the extracted skeletons is described in Fig. 5, consisting of three steps. Based on our Vessel Organization step, the meaningless segments are organized into tree structures with known properties (e.g., leaf depth, leaf parent-child relationship, etc.). This step highly improves the robustness of our method and reduces the labeling error caused by the mislabeling of the tree's root node.

Algorithm 1 Multistencils Fast Marching Skeleton Extraction

Input:
1: $bIMG$, binary image representing vessels.
2: $nIter$, maximum iteration count.
Output:
3: $retLines$, traced vessel skeletons.
4: **function** skeleton((bIMG))
5: $boundDist \leftarrow$ GETBOUNDARYDIST($bIMG$)
6: $(source, maxD) \leftarrow$ MAXDISTPOINT$boundDist$
7: $speedImage \leftarrow boundDist/maxD$
8: **While** $(itt < nIter)$ **do**
9: $(T, Y) \leftarrow$ MSFMspeedImage,source
10: $start \leftarrow$ MAXDISTPOINT(Y)
11: $Line \leftarrow$ SHORTESTPATH$(T, start, source)$
12: $retLines(itt) \leftarrow$ TRIMLINES$(Line)$
13: $itt \leftarrow itt + 1$
14: **end while**
15: **return** $retLines$
16: **end function**

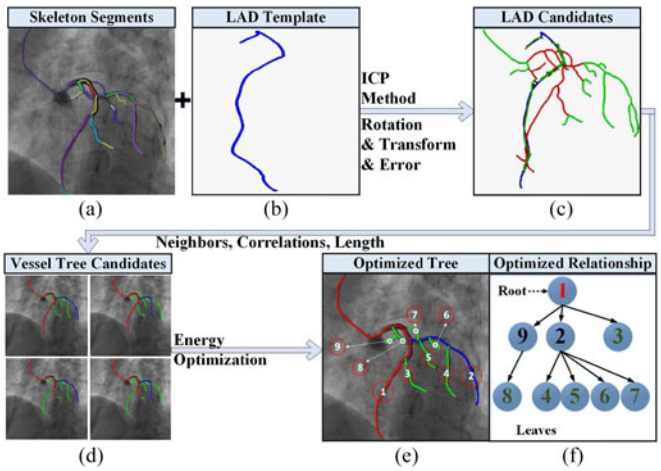

Fig. 5. Pipeline of skeleton organization. (a) Skeleton segments. (b) LAD template. (c) Candidates using LAD. (d) Different organized candidates. (e) and (f) Processed skeletons and their relationship.

A. Two-Dimensional Ground Truth Building

Our prior knowledge comes from a 3-D skeleton model with known labels. Since we are labeling 2-D angiograms, we project the 3-D skeletons onto 2-D images to derive the geometric structure and their relationship according to the viewing angles of the current data set. With the known labels of the 3-D skeleton model, we can easily label the key vessel branches (which we call *landmark*, e.g., LAD, LCX, etc.) on the 2-D projected images. Landmarks at a given angle are shown in Fig. 1, where LAD and LCX are labeled both on 3-D and 2-D projected ground truth images. On the projected images, we call the geometrical and structural information of LAD and LCX as *Template,* and use them for the evaluation in the landmark building step. One LAD template at a given angle is shown in Fig. 5(b).

B. Landmark Building

Obviously, coronary arteries are tree-structured with root, branches, and leaves. It is necessary to identify the root and primary branches to build the entire tree structure. Because of the special characteristics of the vascular angiography, we mainly concentrate our attention on extraction and analysis of three landmarks, the *Catheter*, *LAD* branch, and *LCX* branch by our ICP-based method. The ground truth landmarks at a given angle are shown in Fig. 2.

1) Similarity Term Definition: For landmark building, we focus on extraction of three branches including *Catheter*, *LAD*, and *LCX*. We define ground truth for each branch as G_{CAT}, G_{LAD}, and G_{LCX}, respectively. G_{CAT} is derived from the extraction of beginning images of the sequence, while G_{LAD} and G_{LCX} are from 2-D projected ground truth. We call these three ground truth as *Template,* and use a similarity term to find similar branches from to-be-labeled vessel trees. By denoting *Template* as l, where $l \in \{G_{CAT}, G_{LAD}, G_{LCX}\}$ and each extracted skeleton line segment as s, we define the similarity term $D(l, s)$ based on the results of ICP registration in the extracted image. The $D(l, s)$ is devised to consider structural and geometrical features and evaluated via:

$$D(l,s) = N(l,s)T(l,s)R(l,s)/C(s) \tag{1a}$$

$$N(l,s) = |L(s)/L(l) - 1| + 1 \tag{1b}$$

$$T(l,s) = T_l(s) + \gamma Err_l(s) \tag{1c}$$

$$R(l,s) = 1 + R_l(s)/180 \tag{1d}$$

in which $L(s)$ stands for the length of segment s, $T_l(s)$, $Err_l(s)$, and $R_l(s)$ are parameters calculated for s from ICP with template l, γ is a constant and $C(s)$ stands for the number of points of segment s. Equation (1b) is used to ensure the similar length of labeling and the ground truth segment. Equation (1c) is used to evaluate the transformations in image pairs. Equation (1d) indicates the rotation from labeling to ground truth segments.

2) Catheter Building: In our experiments, the angiograms are taken at the very beginning of the intervention, when the catheter is inside the coronary artery and no contrast agent is injected. Therefore, we can use our vessel extraction method to process the beginning images of the sequence to extract catheter, which is used as ground truth for labeling the catheter branches in the following frames of the sequence.

3) LAD and LCX Building: LAD and LCX branches are even more important than catheter. Once we calculate the $D(l, s)$ for each segment, we obtain the corresponding segments for the template colored in red as shown in Fig. 5(c). Meanwhile, since catheter is directly intervened into LAD branch due to our prior knowledge, we start from the intersection segment and search for the neighbors for each working node, until it is a distal node. As there are multiple distal nodes during search, there are several options that LAD might have. After LAD has been determined, the same procedure advances for the LCX branch. Suppose there are m choices for LAD and n choices for LCX, there are totally $m \times n$ options for the whole combinations. We transform the messy data into vessel trees according to the selected LAD and LCX (See Section V-A), and iterate all the $m \times n$ combinations,

Algorithm 2 ICP-Based Skeleton Segments Organization

Input:
$Cath$, extracted catheter segments.
$LADGr$
$LCXGr$, ground truth for LAD
LCX branch.
$LNodes$, to be labeled segments.
$Coeff$, coefficients between line segments.
Output:
segment combination with minimal energy.
function PROCESSOneImage
    $cathCandi \leftarrow$ ICPLOOKUP($Cath$,$LNodes$)
    $iCath \leftarrow cathCandi$
    $LADCandi \leftarrow$ ICPLOOKUP($LADGr$,$LNodes$)
    $vProcessed \leftarrow$ insert $iCath$
    $LADs \leftarrow$ COLLECTPATHS($LADCandi$,$Coeff$)
    for $m = 0 \rightarrow Count(LADs)$ **do**
        $LCXCandi \leftarrow$ ICPLOOKUP($LCXGr$, $LNodes$)
        $vProcessed \leftarrow$ insert $LADs(m)$
        $LCXs \leftarrow$ COLLECTPATHS ($LCXCandi$,$Coeff$)
        for $n = 0 \rightarrow Count(LCXs)$ **do**
            $vMerged \leftarrow$ MERGE($LADs(m), LCXs(n)$)
            $Energy \leftarrow vesselTreeBP(vMerged)$
        end for
    end for
    $minE, mMin, nMin \leftarrow min(Energy)$
    $sFinal \leftarrow$ MERGE(*LADs(mMin)*, $LCXs(nMin)$)
end function

calculating the globally optimized energy (see Section V-B) for each combination to ensure the robustness of our algorithm. At last, we select the combination with minimal energy as the final structure. The entire computational procedure is described in Algorithm 2.

C. Segments Organization

As soon as the LAD and LCX segments are identified, we can organize rest of the segments clearly, based on the correlation $Corr(p, q)$ between neighboring segments p and q, which is defined as

$$Corr(p,q) = \arctan\left(\frac{|S(p) - S(q)|}{(1 + S(p)S(q))}\right) \tag{2}$$

where $S(p)$ denotes the average slope value for skeleton p, and it is defined as

$$S(p) = \frac{N\sum_{i=1}^{N}(X_p(i)Y_p(i)) - \left(\sum_{i=1}^{N}X_p(i)\right)\left(\sum_{i=1}^{N}Y_p(i)\right)}{N\sum_{i=1}^{N}(X_p(i)X_p(i)) - \left(\sum_{i=1}^{N}X_p(i)\right)\left(\sum_{i=1}^{N}X_p(i)\right)} \tag{3}$$

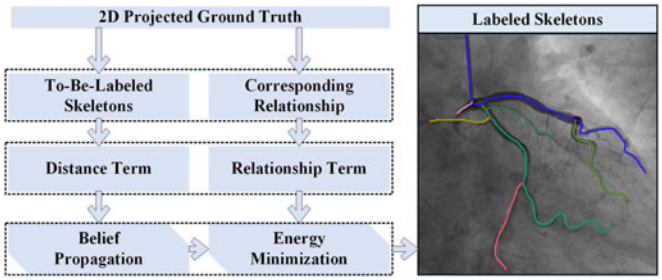

Fig. 6. Pipeline of vessel tree labeling. We define two energy terms to formulate the labeling problem as an energy optimization problem.

where for each skeleton segment p, N denotes the number of points, X_p and Y_p represent the *X*-coordinate and *Y*-coordinate, respectively. In our experiments, once N is smaller than a predefined value, $Corr(p, q)$ is slightly raised to give smaller segments better chances of merging into longer ones.

We start from a random skeleton segment and group neighbors of the current working segment with high correlation recursively. After each group is processed, we continue searching from the other uncovered segments until all segments have been covered. At last, segments belonging to the same group will be merged into a new segment, the points belonging to each old segment will be queued and sorted by its location and the starting point and ending point for this new segment will be refreshed. After the organization, we obtain a totally new structure with more reasonable, continuous segments and skeleton fragments with a reasonable length.

V. Vessel Tree Labeling

After the messy segments have been transformed into well-organized unique tree structures, it is ready to derive the vessel tree (Section V-A) and label the vessels (Section V-B) based on BP as described in Fig. 6.

A. Vessel Tree Building

We build the vessel tree from each organized vessel structures. Each tree node corresponds to a vessel segment in which LAD and LCX correspond to the root node and one of the primary branch respectively. During the construction, we compute the depth, neighborhood, and parent-child relationship for each tree node based on depth-first iteration.

First, we collect the merged skeletons and analyze the key points including bifurcations and distal nodes as input. Second, we build parent-child relationships between segments according to two-tuple (i, p), which indicates that it is a bifurcation point p on segment i. Third, we assign each node with a unique code consisting of the inherent code from its parent and the unique code of itself. This code enables us to compute the minimal path between nodes efficiently. Finally, we shall analyze if the node is a distal node with one bifurcation or an inner node with two bifurcations through looking up the bifurcation table. After all of these analysis, we traverse all nodes in a depth-first manner and record both the depth and the root nodes.

B. Labeling Using BP

We present an energy-based method to analyze the tree-structured vessels robustly with the property of global optimization. The energy term at time t is defined as:

$$E_t(f) = \sum_{p \in P} D_p(f_p) + \lambda \sum_{p,q \in N_p} V_{p,q}(f_p, f_q) \tag{4}$$

where P is the node set of the vessel tree, N_p is the neighboring node set of node p. We define $D_p(f_p)$ as the minimal normalized value that is the same as (1a), which is called by *Distance* term

$$D_p(f_p) = \text{norm}(\min(D(l, f_p))). \tag{5}$$

Meanwhile, we define the $V_{p,q}(f_p, f_q)$ as the *Relationship* term to ensure the continuity between adjacent segments p and q. This term is related to the path length between the node p and its ground truth node f_p. We define $V_{p,q}(f_p, f_q)$ as

$$V_{p,q}(f_p, f_q) = (1 + R_{p,q}(f_p, f_q))(D_p(f_p) + D_q(f_q)) \tag{6}$$

where $R_{p,q}(f_p, f_q)$ denotes the path length from the corresponding ground truth node f_p to node f_q. Since message propagation is processed between neighboring nodes, they have relationships including both parent–child and siblings. Therefore, larger $R_{p,q}(f_p, f_q)$ can easily penalize labels not well fitted with the ground truth.

Once we have the *Distance* and the *Relationship* terms, we find the minimum $E_t(f)$ using BP algorithm, which is comprised of two main steps, message propagation and energy minimization. In the message propagation step, we formulate the message propagated between nodes at the ith iteration as:

$$m^i_{p \to q}(f_q) = \min(\alpha D_p(f_p) + \beta V_{p,q}(f_p, f_q) + \gamma \sum_{s \in N_p \setminus q} m^{i-1}_{s \to p}(f_p)) \tag{7}$$

where α, β, and γ are constants controlling the weights of different components. $N_p \setminus q$ represents all neighbors of segment p except q. We compute the message propagated to neighbor q from each source node p. With a given q, we compute the minimum energy for each p to make the message minimal. After I iterations, we compute the belief vector as

$$b_q(f_q) = D(f_q) + \sum_{p \in N_q} m^I_{p \to q}(f_q). \tag{8}$$

After obtaining the energy term at t, we use the temporal information to ensure the continuity between frames within the same sequence. We define the energy term as

$$E(f) = (1 - \eta) E_t(f) + \eta E_{t-1}(f) \tag{9}$$

where η is a parameter controlling the strength of continuity between frame t and frame $t - 1$. Eventually, we compute the minimum sum of all grouped vessel skeleton segments and obtain the optimal solution for $E(f)$. $E_{t-1}(f)$ is the labeling state of last frame and the method proceeds for the next frame until we arrive at the end of the sequence.

Our algorithm is robust for incomplete data due to its global optimization nature. Most classical methods proposed before are based on feature extraction and matching, while some others improve the matching method by using iterating techniques or coarse-to-fine techniques to enhance the robustness. However, the intrinsic nature of these methods has undoubtedly given rise to the low efficiency for handling blurry and incomplete imaging data, since they can not guarantee the globally-optimized results. Our method could automatically overcome these difficulties, because it is not based on classical geometrical feature matching but is rooted in the energy optimization theory which can achieve global-optimized result. It may be noted that, we do not apply feature matching directly, but formulate features as energy terms and spread the message of the term using BP which enables to achieve the correct labeling results even when features are not precise in the first place.

TABLE I
LABELING STATISTICS

	Labeling Accuracy (correct/extracted count)				
Image Count	CAT	LAD	LCX	OM	D
1770	1770/1770 100.0%	1405/1429 98.3%	1344/1368 98.2%	953/1006 94.7%	1101/1126 97.8%

VI. EXPERIMENTS AND VALIDATION

We use X-ray angiograms from 19 persons, each comprising several data sets from different view angles to validate both the correctness and the robustness of our method, best suited for handling blurry and incomplete data. Each data set at a single view consists of at least forty images.

We have shown some typical cases for robustness validation. Meanwhile, labeling statistics are described in Table I for whole data set. Due to page limit, detailed information for each data set are described in the supplementary material. According to the statistics, All catheter branches are extracted correctly from the original angiograms. Incorrectly-labeled LAD and LCX branches are mainly caused by the blurry or overlapping problems. Incorrectly-labeled OM branches are mainly distributed in some typical sets, where OM and other branches are overlapped because of the viewing angles. It is also the same reason for D branches.

Data Acquisition. Among all the procedures, we use clinical data captured by a Philip single-plane X-ray machine. The system setup and view angles in X-ray angiography are illustrated in Fig. 7. We use four parameters (D_{I2H}, D_{O2H}, θ_H, θ_V, also described in Fig. 7) to represent the intrinsic and external state during imaging.

Robustness Validation. The robustness of our method mainly lies in two aspects: its ability to extract well-structured vessel trees when handling blurry images, and its robustness for obtaining correct labeling results on incomplete data.

First, cases for blurry angiograms are given in Fig. 8(a) (low contrast, blurry), Fig. 8(b) (low contrast, vessel narrowness), Fig. 9(a) (blurry, organs), Fig. 9(d) (blurry, vessel narrowness), and Fig. 10(a) (blurry). Blurry images are usually caused because of the vessels' narrowness or the shortage of contrast

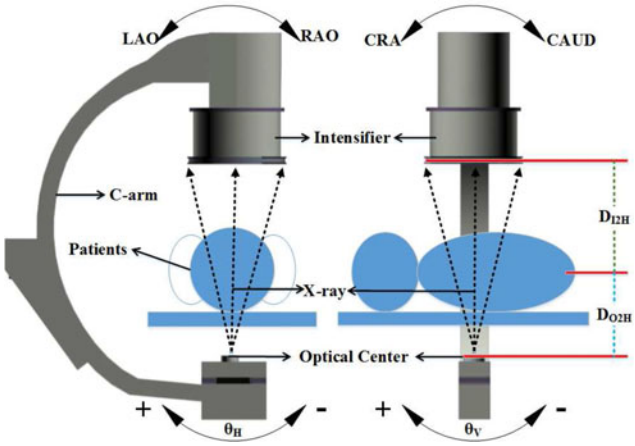

Fig. 7. Illustrative sketches for X-ray intrinsic parameters. D_{I2H} and D_{O2H} represent the distance from intensifier to patient and from optical center to patient, respectively. θ_V and θ_H are angles the C-arm rotates in space. LAO and CRA are defined as positive angles, while RAO and CAUD are defined as negative angles along their corresponding axes.

agent. Also, images in Fig. 8(c) (spines captured), Fig. 8(d) (spines, pulmonary, severe artifacts), Fig. 9(b) (spines, pulmonary), Fig. 9(b) (spines, pulmonary), Fig. 9(c) (spines, pulmonary, ribs), Fig. 10(b) (spines, vessel narrowness), Fig. 10(c) (spines, pulmonary), and Fig. 10(d) (ribs) denote another problem that artifacts as well as other organs are captured in angiograms. The experiments above have shown that our method can handle images of low quality and still extract correct vessel structures and labels.

Second, in Figs. 8–10, we have shown results during contrast injection. At the beginning of each subfigure, although the entire cardiovascular structure has not been contrasted since the contrast agent is being injected, our method can figure out exact labels from current incomplete structures. The temporal information from the previous frame also helps derive the correct labels from incomplete data.

Therefore, even though with images of low quality (blurry, organs, etc.) or incomplete data (incomplete vascular structures during contrast injection), our method can still have the capability of deriving correct, coherent results; hence, demonstrating its overall robustness due to its global optimization nature and the utility of temporal information.

Preprocessing and Labeling. Preprocessing and labeling results are documented in Figs. 8–10. The first row indicate the original angiograms with extracted coronary artery trees organized in different colors. Skeletons in *Red* indicate they are root skeletons and they are more likely the LAD branches. Skeletons in *blue* indicate more likely the LCX branches. Skeletons in *Green* indicate they are side branches. Original tree structures are one pixel width but they are expanded and drawn in a visible way (i.e., becoming thicker) to make them clear. The second row indicates the labeled vessels. We evaluate major branches including *LAD, LCX, OM,* and *D* to validate the correctness.

Performance. The performance of our proposed method is documented in Fig. 14. We use different legends to represent the different procedures of our method. Besides, performance figure is attached to each data set in the supplementary material. Totally, the processing time reaches maximum at 4 s and is around 2 s in most cases. Therefore, although our method is composed of several steps, the performance is reasonable according to our statistics.

Comparison. Mukherjee and Gopi [33] proposed an iterative method to look for the similarities between geometric trees, based on the features whose efficiency greatly relies on feature extraction. Chalopin *et al.* [34] proposed a coarse-to-fine search method and the matching quality in the following steps highly relies on prior results. Similar methods may have considered geometrical or feature similarities, which are not robust enough to handle blurry, low-quality, or even incomplete images. In sharp contrast, our method is based on the rigorous theory of energy optimization and its powerful numerical solvers; hence, capable of obtaining optimized results that guarantee the robustness to the greatest extend. The experiments and results have shown that, our method can extract and label the vessel tree structure well for both clear and blurry images.

Discussions. This paper has detailed a robust method comprising several steps for vessel labeling. The necessity of each step lies in the strong requirements for both data simplification and assuring the robustness of our method. Since the coronary artery labeling for X-ray is a very specific subject for medical image analysis, we have not found reasonable and comprehensive performance statistics in other publications. Nevertheless, to our best knowledge, we have validated our method on the largest experiment data set (with 39 data sets from 19 persons, totally 1770 X-ray angiograms) in this area, and the achieved results have shown the robustness and correctness of our method. Beside, the maximum processing time is 4169.7 ms, minimum is 1411.1 ms, and average is 2733.9 ms, which are reasonable and adequate for both research and clinical uses.

Limitations. Although our method has achieved robust results, there are still certain shortcomings due to low quality of the images. Due to dynamic movements of heart, the imaging quality is very poor, unavoidably causing severe artifacts if the contrast agent is not injected steadily, and unfortunately, this scenario is extremely challenging for all the cardiovascular processing methods. To improve the overall performance in this situation, we intend to integrate our method with user interaction to combat severe artifacts, and it is also possible to enhance the efficiency of our method.

VII. Applications

Our efficient method can be easily applied for the analysis and diagnosis tasks relevant to heart disease. We have conducted three more applications to validate the correctness and scalability of our method.

Vessel Diameter Estimation and Analysis. The diameter of vessels is an important indicator for disease, especially for heart-related diseases, such as vessel stenosis. Collecting and analyzing diameters from the X-ray images affords strong basis for doctors' diagnosis. In our application, we collect the diameters for all the extracted vessels and provide reasonable advice and assistance for diagnosis by calculating the distance map on binary images. We analyze the diameters and seek nodes

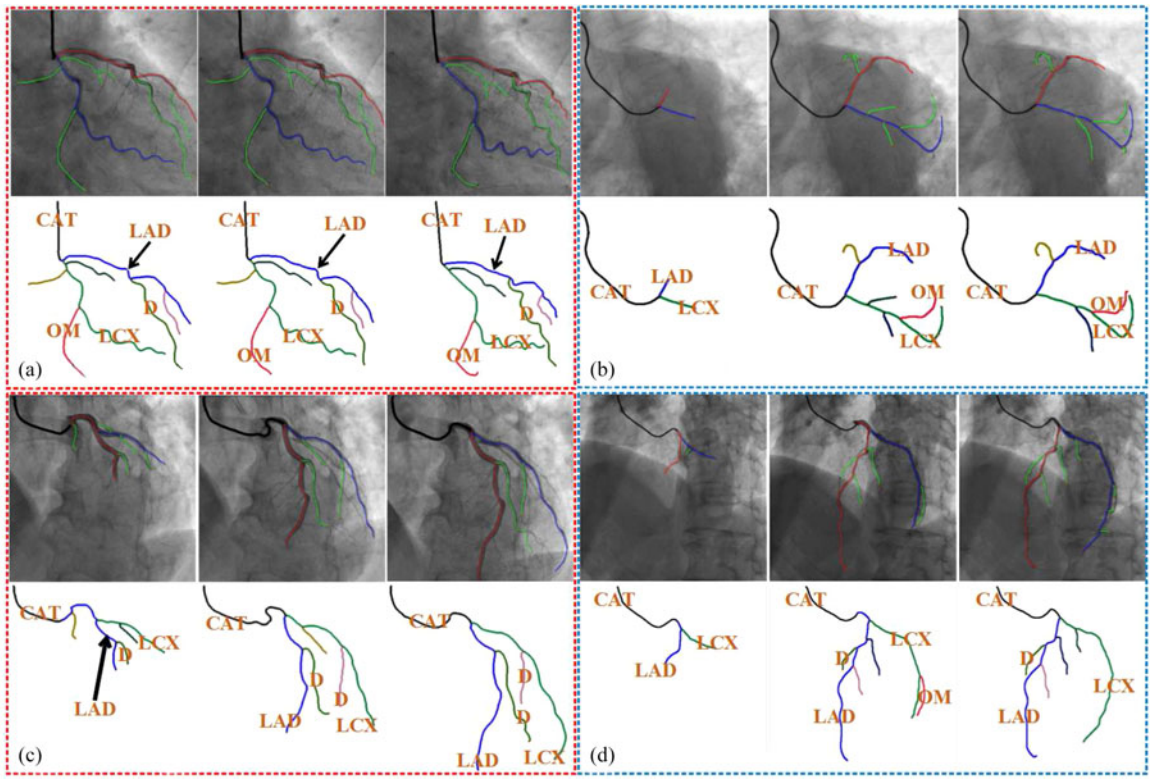

Fig. 8. Extraction and labeling results. Note that, the original skeletons are of only one pixel width and are expanded for better visualization. For every image, top row: tree structures; bottom row: labeling results. (a) RAO28CAU20, (b) LAO42CAU34, (c) LAO31XRA27, LAO37CRA26.

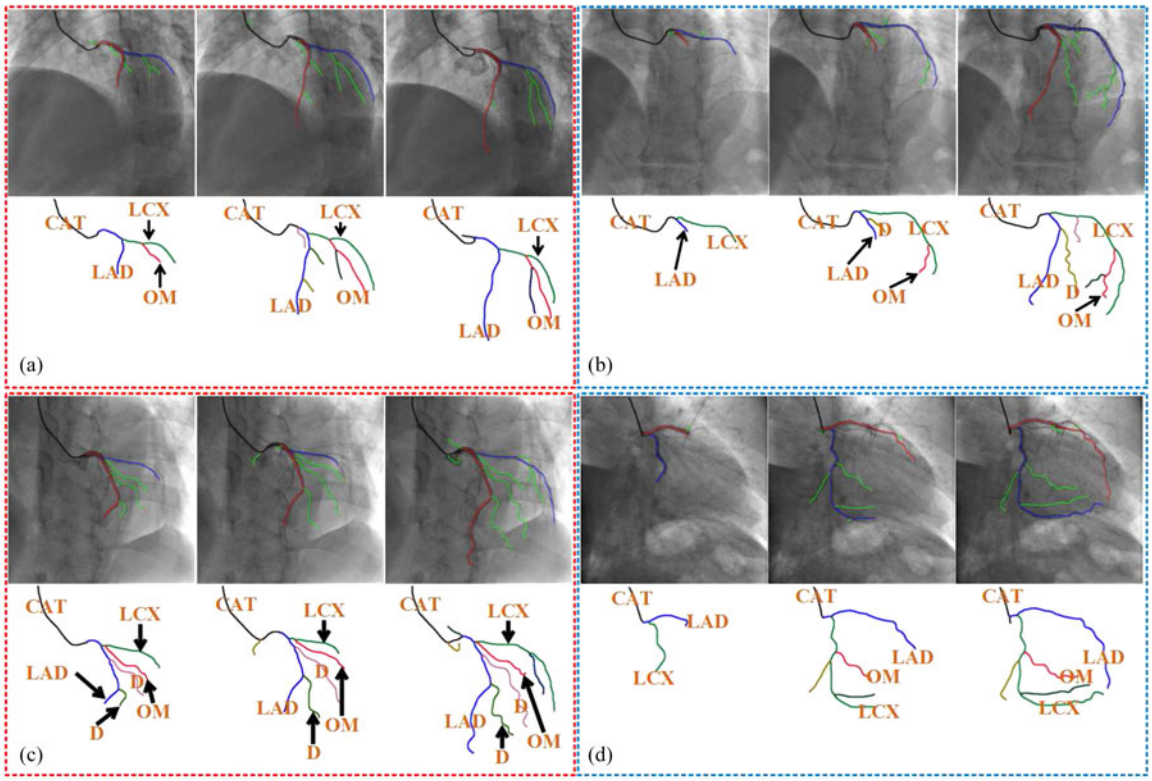

Fig. 9. Extraction and labeling results. On the top row of each subfigure, red segments: primary branches; blue segments: secondary branches; green segments: side branches. Bottom row: labeling results. (a) LAO33CRA25, (b) LAO31CRA24, (c) LAO35CRA22, RAO36CAU21.

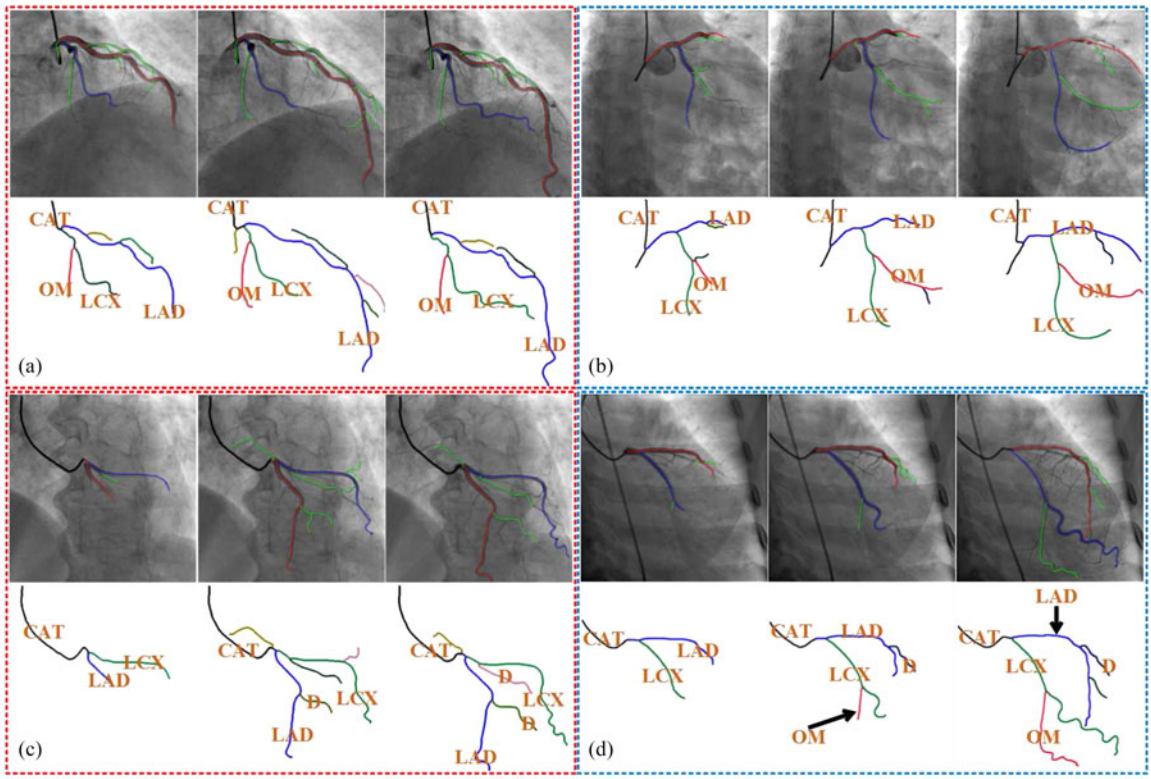

Fig. 10. Extraction and labeling results. All images have shown severe artifacts, demonstrating the robustness of our method through strong visual effects.

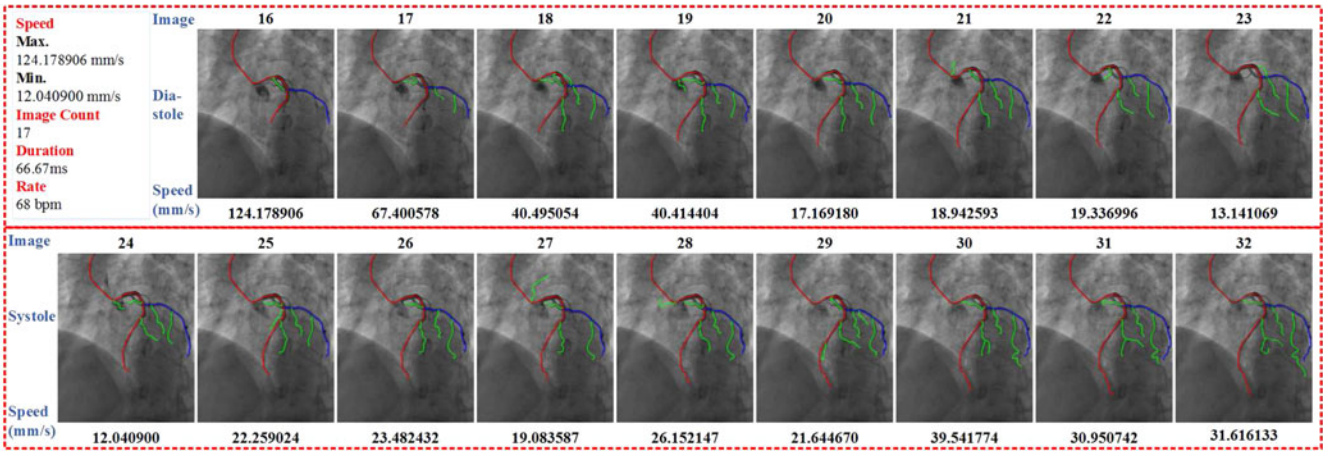

Fig. 11. One traced cardiac cycle consisting of 17 images. The rate is close to the standard value.

whose diameters are abnormal compared with their neighbors. We provide the numerical analysis as well as the visual analysis for better diagnosis. We have shown some stenosis prediction results in Fig. 13. We use hollow circles to indicate vessels whose diameters change severely. Larger circles indicate more severe changes and should attract more attention from doctors. Nine images from different data sets are shown, while six of them are enlarged to give a better view on the diameter visualization.

Flow-Velocity Estimation and Analysis. The flow velocity of coronary arteries is also an significant indicator for many heart-related disease. State-of-the-art methods collecting flow-velocity statistics are mainly based on the measurements from medical instrumentations, making it complicated and hard to be operated, sometimes not accurate either. The starting point of this application is to select those patients, who probably have stenosis with irregular blood flow speed. In our application, we label frame t and frame $t+1$ in the same sequence based on our proposed method so that we can obtain the corresponding structure $S_t(p)$ and $S_{t+1}(f_p)$ in adjacent frames. Based on these corresponding structures, we can compute the changes of movements between frames, enabling us to compute both the instantaneous movement speed for each segment and the

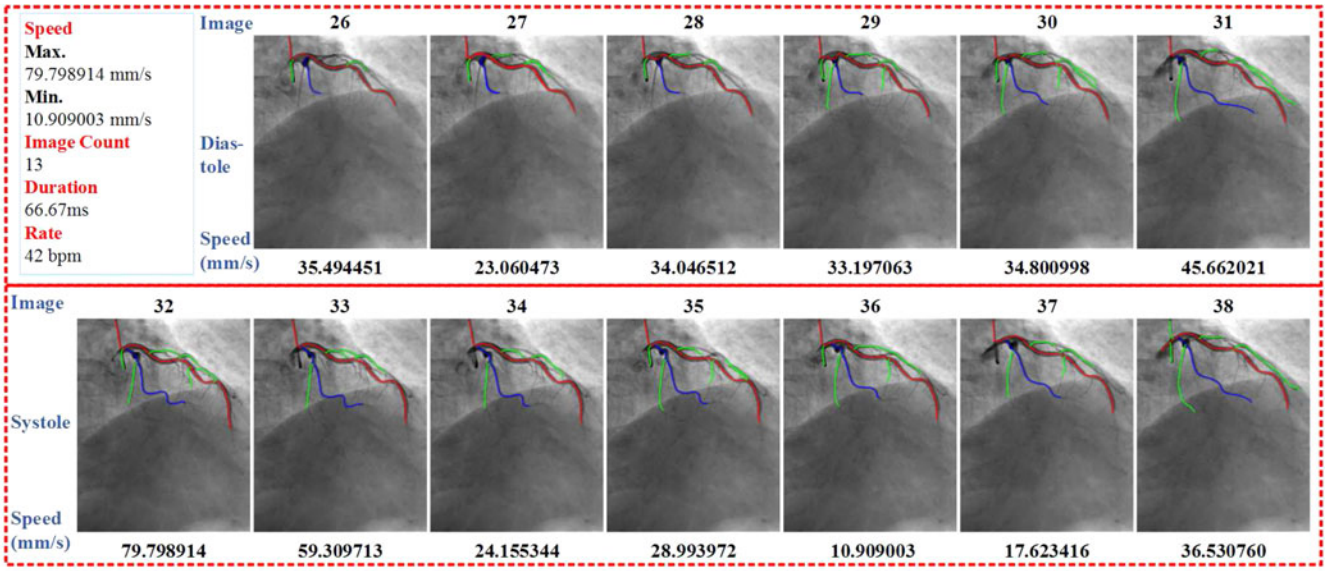

Fig. 12. One traced cardiac cycle consisting of thirteen images. The rate is only 42 b/m. This patient may be suffering from irregular heart rhythm or even bradycardia based on diagnosis from our extracted rate.

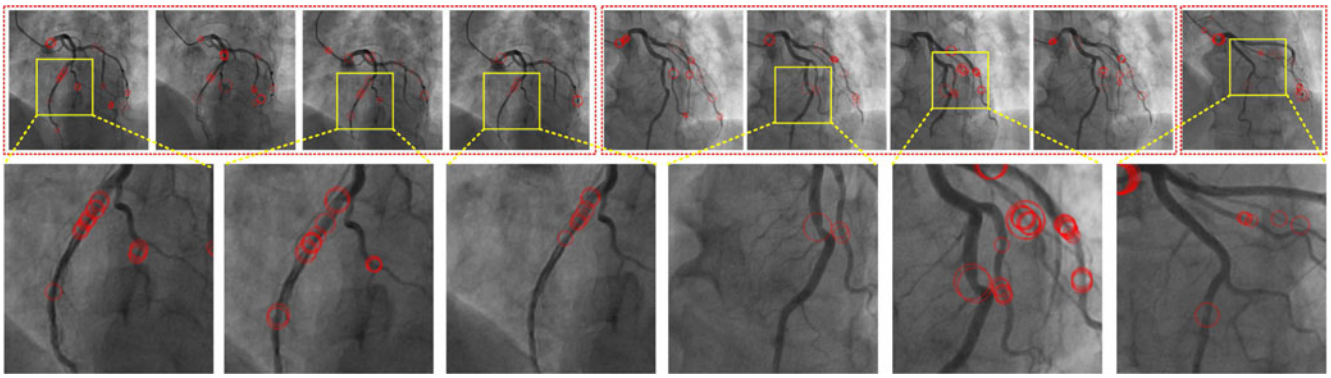

Fig. 13. Stenosis prediction based on diameter analysis. Larger circles indicate more severe diameter changes. Six out of nine images have been enlarged to give a better visualization on diameter.

average speed for the whole structures. We have shown some results for flow-speed estimation in Figs. 11 and 12. Statistical parameters related to flow speed are shown separately in each figure including the minimum and maximum speed. Instant speed for each image is labeled in the bottom row in mm/s.

Heart Beat Rate Estimation and Analysis. The state-of-art methods for X-ray angiograms will always require the cardiogram synchronized with the image sequences to explicitly identify the corresponding images among different sequences, which unavoidably increases the requirements and limits the applicability. In our application, we calculate the weighted average distance from each skeleton segment s to other segments. Longer segments will have larger weights. With frames at time t and time $t+1$, we shall seek corresponding vessel structures between adjacent frames using our method. By comparing the distance $M_t(s)$ and $M_{t+1}(f_s)$, we obtain the movement trend of each vessel tree node between the adjacent frames in the same sequence, and determine if the coronary arteries are at the relaxation or contraction stage. If $M_{t+1}(f_s) > M_t(s)$ repeatedly, it is justified as diastole, otherwise it is systole. We can automatically extract the systole period and diastole period in the sequence. We have also tested heart beat estimation as shown in Figs. 11 and 12, where we derive the number of images of one cardiac cycle, duration of each image, and the heart rate as tracking parameters. The heart rate is counted in *bpm* meaning *beat per minute* and the flow speed is in *mm/s*. The heart rate in Fig. 11 is close to the standard value 75 b/m, while Fig. 12 has a heart rate much lower than the standard value, indicating that the patient may suffer noisy heart rhythm and even bradycardia if this situation continues to repeat.

VIII. Conclusion

We have developed a novel coronary artery labeling system from X-ray angiograms. The uniqueness of our system is its simultaneous handling on labeling, as well as various applications

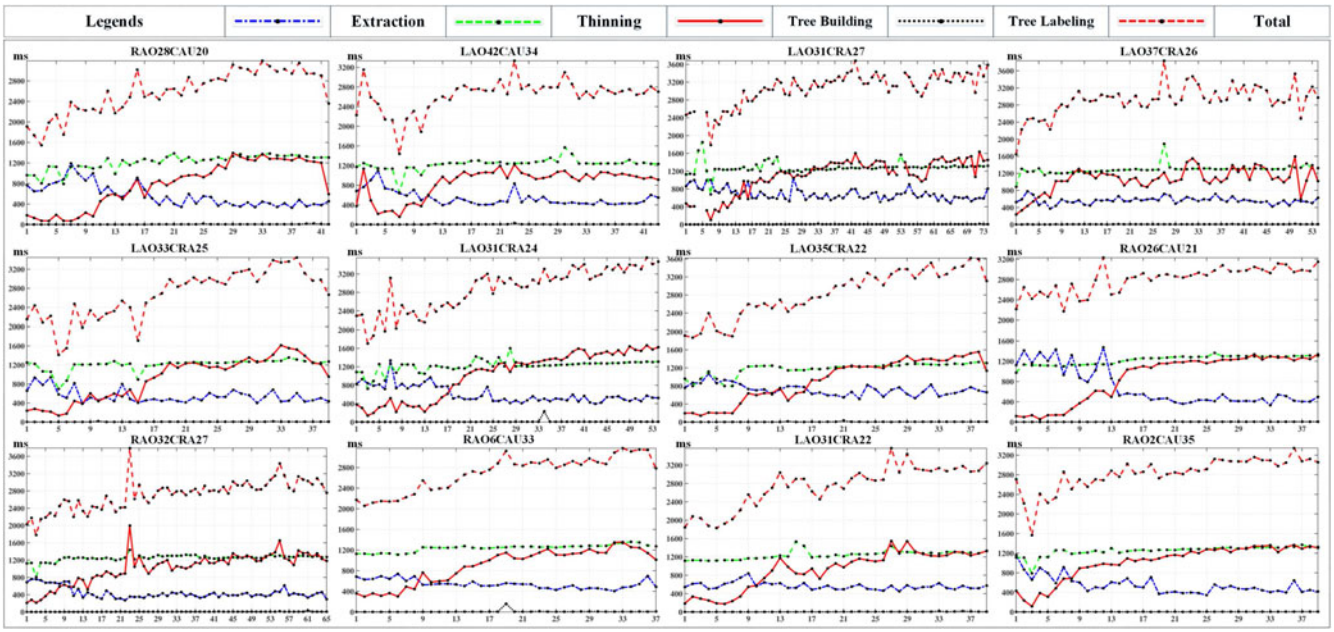

Fig. 14. Performance in all of our data sets. Legends have been given to help document time consumption for each step. The thinning method is always time consuming and costs nearly half of the total time. The extraction step is very fast because of its GPU acceleration.

for physiological parameter extraction. The critical technical components of our system include the robust global optimization formulation for vessel labeling and the parallel algorithms supporting great performance and robustness. At the stage of vessel tree building, our system has the capability of transforming the extracted messy, unorganized segments into well-organized tree structures. At the labeling stage, we formulate the labeling problem using an energy optimization approach solved by BP without the need of explicit feature extraction, registration, and tracking. Besides, we had explored three applications to highlight the usefulness as well as the possible generalization of our method. The experimental results have shown that our method is robust to noise and even incomplete data mainly because of the algorithms' global optimization nature. Our immediate goal in our ongoing and upcoming work is to continue to improve the system's performance and expand its functionalities towards clinic trial in the near future.

ACKNOWLEDGMENT

This work is supported in part by the National Natural Science Foundation of China under Grant 61190120, Grant 61190121, Grant 61190125, Grant 61532002, Grant 61300068, and Grant 61300067, the National Science Foundation of USA under Grant IIS-0949467, Grant IIS-1047715, and Grant IIS-1049448), the National High Technology Research and Development Program (863 Program) of China under Grant 012AA011503, and the Postdoctoral Science Foundation of China under Grant 2013M530512.

REFERENCES

[1] V. Vezhnevets and V. Konouchine, "Growcut: Interactive multi-label N–D image segmentation by cellular automata," in *Proc. GraphiCon*, 2005, pp. 150–156.

[2] Y. Boykov, O. Veksler, and R. Zabih, "Fast approximate energy minimization via graph cuts," *IEEE Trans. Pattern Anal. Mach. Intell.*, vol. 23, no. 11, pp. 1222–1239, Nov. 2001.

[3] Z. Zhang, " Iterative point matching for registration of free-form curves and surfaces," *Int. J. Comput. Vis.*, vol. 13, no. 2, pp. 119–152, 1994.

[4] P. A. Heidenreich, J. G. Trogdon, O. A. Khavjou, J. Butler, K. Dracup, M. D. Ezekowitz, E. A. Finkelstein, Y. Hong, S. C. Johnston, A. Khera et al.,, "Forecasting the future of cardiovascular disease in the united states a policy statement from the american heart association," *Circulation*, vol. 123, no. 8, pp. 933–944, 2011.

[5] V. Roger, A. Go, D. Lloyd-Jones, R. Adams, J. Berry, T. Brown, M. Carnethon, S. Dai, G. de Simone, E. Ford *et al.*, "AHA statistical update: Heart disease and stroke statistics—2011 update," *Circulation*, vol. 123, pp. e18–e209, 2011.

[6] "Registry of births and deaths 2011: Singapore demographic bulletin." Immigration & Checkpoints Authority, Singapore, 2012.

[7] J. J. Heys, N. Holyoak, A. M. Calleja, M. Belohlavek, and H. P. Chaliki, "Revisiting the simplified Bernoulli equation," *Open Biomed. Eng. J.*, vol. 4, pp. 123–128, 2010.

[8] A. F. Frangi, W. J. Niessen, K. L. Vincken, and M. A. Viergever, "Multiscale vessel enhancement filtering," in *Proc. Med. Image Comput. Comput. Assisted Intervention*. New York, NY, USA: Springer, 1998, pp. 130–137.

[9] C. Kirbas and F. Quek, "A review of vessel extraction techniques and algorithms," *ACM Comput. Surveys*, vol. 36, no. 2, pp. 81–121, 2004.

[10] A. Salazar-Gonzalez, D. Kaba, Y. Li, and X. Liu, "Segmentation of the blood vessels and optic disk in retinal images," *IEEE J. Biomed. Health Inform.*, vol. 18, no. 6, pp. 1874–1886, Nov. 2014.

[11] A. Hoover, V. Kouznetsova, and M. Goldbaum, "Locating blood vessels in retinal images by piecewise threshold probing of a matched filter response," *IEEE Trans. Med. Imag.*, vol. 19, no. 3, pp. 203–210, Mar. 2000.

[12] Q. Li, J. You, and D. Zhang, "Vessel segmentation and width estimation in retinal images using multiscale production of matched filter responses," *Exp. Syst. Appl.*, vol. 39, no. 9, pp. 7600–7610, 2012.

[13] A.-P. Condurache and T. Aach, "Vessel segmentation in angiograms using hysteresis thresholding," in *Proc. IAPR Conf. Mach. Vis. Appl.*, 2005, pp. 269–272.

[14] B. Zhang, L. Zhang, L. Zhang, and F. Karray, "Retinal vessel extraction by matched filter with first-order derivative of gaussian," *Comput. Biol. Med.*, vol. 40, no. 4, pp. 438–445, 2010.

[15] T. Y. Zhang and C. Y. Suen, "A fast parallel algorithm for thinning digital patterns," *Commun. ACM*, vol. 27, no. 3, pp. 236–239, 1984.

[16] R. Van Uitert and I. Bitter, "Subvoxel precise skeletons of volumetric data based on fast marching methods," *Med. Phys.*, vol. 34, no. 2, pp. 627–638, 2007.

[17] M. S. Hassouna and A. A. Farag, "Multistencils fast marching methods: A highly accurate solution to the Eikonal equation on cartesian domains," *IEEE Trans. Pattern Anal. Mach. Intell.*, vol. 29, no. 9, pp. 1563–1574, Sep. 2007.
[18] N. Ezquerra, S. Capell, L. Klein, and P. Duijves, "Model-guided labeling of coronary structure," *IEEE Trans. Med. Imag.*, vol. 17, no. 3, pp. 429–441, Jun. 1998.
[19] K. Haris, S. Efstratiadis, N. Maglaveras, C. Pappas, J. Gourassas, and G. Louridas, "Model-based morphological segmentation and labeling of coronary angiograms," *IEEE Trans. Med. Imag.*, vol. 18, no. 10, pp. 1003–1015, Oct. 1999.
[20] G. Yang, A. Broersen, R. Petr, P. Kitslaar, M. de Graaf, J. Bax, J. Reiber, and J. Dijkstra, "Automatic coronary artery tree labeling in coronary computed tomographic angiography datasets," in *Proc. Comput. Cardiol.*, Sep. 2011, pp. 109–112.
[21] S. Geman and D. Geman, "Stochastic relaxation, gibbs distributions, and the Bayesian restoration of images," *IEEE Trans. Pattern Anal. Mach. Intell.*, vol. PAMI-6, no. 6, pp. 721–741, Nov. 1984.
[22] J. D. Lafferty, A. McCallum, and F. C. N. Pereira, "Conditional random fields: Probabilistic models for segmenting and labeling sequence data," in *Proc. 18th Int. Conf. Mach. Learn.*, San Francisco, CA, USA, 2001, pp. 282–289.
[23] J. Pearl, "Reverend bayes on inference engines: A distributed hierarchical approach," in *Proc. Amer. Assoc. Artif. Intell. Nat. Conf.*, 1982, pp. 133–136.
[24] R. Szeliski, R. Zabih, D. Scharstein, O. Veksler, V. Kolmogorov, A. Agarwala, M. Tappen, and C. Rother, "A comparative study of energy minimization methods for Markov random fields with smoothness-based priors," *IEEE Trans. Pattern Anal. Mach. Intell.*, vol. 30, no. 6, pp. 1068–1080, Jun. 2008.
[25] B. Potetz and T. S. Lee, "Efficient belief propagation for higher-order cliques using linear constraint nodes," *Comput. Vis. Image Understanding*, vol. 112, no. 1, pp. 39–54, 2008.
[26] Y. Y. Boykov and M.-P. Jolly, "Interactive graph cuts for optimal boundary & region segmentation of objects in N-D images," in *Proc. 8th IEEE Int. Conf. Comput. Vis.*, 2001, vol. 1, pp. 105–112.
[27] V. Kolmogorov and R. Zabin, "What energy functions can be minimized via graph cuts?" *IEEE Trans. Pattern Anal. Mach. Intell.*, vol. 26, no. 2, pp. 147–159, Feb. 2004.
[28] C. Rother, V. Kolmogorov, and A. Blake, "Grabcut: Interactive foreground extraction using iterated graph cuts," in *Proc. ACM Trans. Graph.*, vol. 23, no. 3, pp. 309–314, 2004.
[29] X. Liu, F. Hou, A. Hao, and H. Qin, " A parallelized 4D reconstruction algorithm for vascular structures and motions based on energy optimization," *Visual Comput.*, vol. 31, pp. 1–16, 2014.
[30] Y. Onishi, K. Aoki, K. Amaya, T. Shimizu, H. Isoda, Y. Takehara, H. Sakahara, and T. Kosugi, "Accurate determination of patient-specific boundary conditions in computational vascular hemodynamics using 3D cine phase-contrast MRI," *Int. J. Numerical Methods Biomed. Eng.*, vol. 29, no. 10, pp. 1089–1103, 2013.
[31] Z.-U. Rahman, D. J. Jobson, and G. A. Woodell, "Multi-scale retinex for color image enhancement," in *Proc. Int. Conf. Image Process.*, 1996, vol. 3, pp. 1003–1006.
[32] J. A. Bærentzen, "On the implementation of fast marching methods for 3D lattices," in *Informatics and Mathematical Modelling*, Tech. Univ. Denmark, Denmark, Tech. Rep. IMM-TR-2001-13, 2001.
[33] U. Mukherjee and M. Gopi, "Finding feature similarities between geometric trees," in *Pacific Graphics Short Papers*, J. Keyser, Y. J. Kim, and P. Wonka, Eds. Geneva, Switzerland: The Eurographics Association, 2014.
[34] C. Chalopin, I. Magnin, and G. Finet, "Automatic labeling of the coronary tree using a three dimensional reference prior model," in *Proc. Comput. Cardiol.*, Sep. 1998, pp. 761–764.

Xinglong Liu received the bachelor's degree in computer science from Yantai University, Yantai, China, in 2010. He is currently working toward the Ph.D. degree in the State Key Laboratory of Virtual Reality Technology and Systems at Beihang University, Beijing, China.

His research interests include 3-D modeling, reconstruction, and medical image processing.

Fei Hou received the Ph.D. degree in computer science from Beihang University, Beijing, China, in 2012.

He is currently a Research Fellow at Nanyang Technological University, Singapore. His research interests include medical image processing, image-based modeling, and data vectorization etc.

Hong Qin received the B.S. and M.S. degrees in computer science from Peking University, Beijing, China, the Ph.D. degree in computer science from the University of Toronto (UofT), Toronto, ON, Canada, in 1995.

He is currently a Full Professor of computer science in the Department of Computer Science, Stony Brook University, NY, USA. During his years at the UofT, he received UofT Open Doctoral Fellowship. He also received NSF CAREER Award from the US National Science Foundation, Honda Initiation Award, and Alfred P. Sloan Research Fellow by the Sloan Foundation. Currently, he is an Associate Editor for *The Visual Computer, Graphical Models*, and *Journal of Computer Science and Technology*. His research interests include geometric and solid modeling, graphics, physics-based modeling and simulation, computer-aided geometric design, human–computer interaction, visualization, and scientific computing.

Dr. Qin is a Senior Member of the IEEE and the IEEE Computer Society.

Aimin Hao was born in 1968, he received the Ph.D. degree in computer science from Beihang University, Beijing, China, in 2006. He is currently a Professor of Computer School, Beihang University, and a Vice Director of State Key Laboratory at Virtual Reality Technology and Systems. His research interests include virtual reality, database application, and information system development.